JOURNAL OF BACTERIOLOGY, Mar. 2008, p. 1518–1530 Vol. 190, No. 5
0021-9193/08/$08.00+0 doi:10.1128/JB.01640-07

Differential Role of Ferritins in Iron Metabolism and Virulence of the Plant-Pathogenic Bacterium *Erwinia chrysanthemi* 3937[▽]

Aïda Boughammoura,[1] Berthold F. Matzanke,[2] Lars Böttger,[3] Sylvie Reverchon,[4] Emmanuel Lesuisse,[5] Dominique Expert,[1] and Thierry Franza[1]*

Laboratoire des Interactions Plantes Pathogènes, UMR 217 INRA/UMPC/AgroParisTech, 16 rue Claude Bernard, 75005 Paris, France[1]; Isotopenlabor der TNF, Universität zu Lübeck, Ratzeburger Allee 160, D-23538 Lübeck, Germany[2]; Institut für Physik, Universität zu Lübeck, Ratzeburger Allee 160, D-23538 Lübeck, Germany[3]; Unité de Microbiologie et Genetique, UMR CNRS/INSA/UCB 5122, 69622 Villeurbanne, France[4]; and Laboratoire d'Ingénierie des Protéines et Contrôle Métabolique Institut Jacques Monod/CNRS/Universités Paris 6 and 7, 2 place Jussieu, 75251 Paris Cedex 05, France[5]

Received 10 October 2007/Accepted 17 December 2007

During infection, the phytopathogenic enterobacterium *Erwinia chrysanthemi* has to cope with iron-limiting conditions and the production of reactive oxygen species by plant cells. Previous studies have shown that a tight control of the bacterial intracellular iron content is necessary for full virulence. The *E. chrysanthemi* genome possesses two loci that could be devoted to iron storage: the *bfr* gene, encoding a heme-containing bacterioferritin, and the *ftnA* gene, coding for a paradigmatic ferritin. To assess the role of these proteins in the physiology of this pathogen, we constructed ferritin-deficient mutants by reverse genetics. Unlike the *bfr* mutant, the *ftnA* mutant had increased sensitivity to iron deficiency and to redox stress conditions. Interestingly, the *bfr ftnA* mutant displayed an intermediate phenotype for sensitivity to these stresses. Whole-cell analysis by Mössbauer spectroscopy showed that the main iron storage protein is FtnA and that there is an increase in the ferrous iron/ferric iron ratio in the *ftnA* and *bfr ftnA* mutants. We found that *ftnA* gene expression is positively controlled by iron and the transcriptional repressor Fur via the small antisense RNA RyhB. *bfr* gene expression is induced at the stationary phase of growth. The σ^S transcriptional factor is necessary for this control. Pathogenicity tests showed that FtnA and the Bfr contribute differentially to the virulence of *E. chrysanthemi* depending on the host, indicating the importance of a perfect control of iron homeostasis in this bacterial species during infection.

Erwinia chrysanthemi 3937, now called *Dickeya dadantii*, is a pathogenic enterobacterium that is able to cause soft rot diseases in a wide range of economically important crops (49, 55). The soft rot symptom produced by *E. chrysanthemi* consists of a progressive disorganization of parenchymatous tissues called maceration and results from several bacterial enzymatic activities, including pectinases and endoglucanases, which work in concert to degrade plant cell walls (43). The bacteria colonize the intercellular spaces of leaves and progress intercellularly to invade the other aerial parts of the plant (40). Under these conditions, *E. chrysanthemi* cells encounter an oxidative environment, as plant tissues produce active oxygen species in response to microbial attack (16). Active protective systems against oxidative damages, such as the methionine sulfoxide reductase MsrA and the manganese-containing superoxide dismutase, are essential for the outcome of the infection (13, 50). The production of the siderophores chrysobactin and achromobactin, two iron scavengers, is also essential for *E. chrysanthemi* cells to cause a systemic infection (14, 15, 19). Therefore, during the infectious process, a tight control of the intracellular iron content is important. Indeed, the redox properties of iron, which make this metal a valuable cofactor in a multitude of cellular process, can also lead to the production of harmful radicals. For instance, ferrous iron can exacerbate the oxidative stress through Fenton's reaction, which generates the highly toxic and reactive hydroxyl radical OH· (23, 30). We have demonstrated that the transcriptional repressor Fur, which controls the intracellular iron concentration, is involved in the pathogenicity of strain 3937 (18). The importance of the connection between iron metabolism and oxidative stress during the early steps of infection by *E. chrysanthemi* was emphasized with the discovery that the Suf machinery encoded by the *sufABCDSE* operon participates in the formation of Fe-S clusters under iron starvation and oxidative conditions and is necessary for full virulence (41, 42). The other mechanisms involved in the control of iron homeostasis during infection are currently not known.

In many bacteria, the removal of an excess of ferrous iron by its subsequent oxidation is achieved by ferritins or ferritin-like proteins. Ferritins constitute a broad superfamily of iron storage proteins, widespread in all domains of life, in aerobic or anaerobic organisms (3, 37). These proteins fall into three classes: ferritins that are heme free, found in pro- and eukaryotes, heme-containing bacterioferritins, found only in bacteria, and Dps proteins (DNA protein from starved cells), now called miniferritins, present only in prokaryotes (11, 52). They are composed of 24 identical subunits for ferritins and bacterioferritins and 12 identical subunits for the Dps proteins. These subunits assemble to make a spherical protein shell surrounding a central cavity able to hold up to 2,000 to 3,000

* Corresponding author. Mailing address: Laboratoire des Interactions Plantes Pathogènes, UMR 217 INRA/UMPC/AgroParisTech, 16 rue Claude Bernard, 75005 Paris, France. Phone: (33) 1 44 08 72 30. Fax: (33) 1 44 08 16 31. E-mail: franza@inapg.fr.

▽ Published ahead of print on 28 December 2007.

TABLE 1. Bacterial strains, bacteriophage, and plasmids used in this study

Strain, phage, or plasmid	Relevant characteristic(s)	Source or reference
Strains		
Erwinia chrysanthemi		
3937	Wild type isolated from African violet	Our collection
L2	Lac$^-$ derivative of 3937	21
PPV40	*ftnA*Ω-*spec* FtnA$^-$ Spec^r	This work
PPV41	*ftnA*::*uidA* FtnA− Km^r	This work
PPV39	*fur*Ω-*spec* Fur$^-$ Spec^r	18
PPV42	*ftnA*::*uidA fur*Ω-*spec* FtnA$^-$ Fur$^-$ Km^r Spec^r	This work
PPV43	*bfr*Ω-*Km* Bfr$^-$ Km^r	This work
PPV44	*bfr*::*uidA* Bfr$^-$ Km^r	This work
A4109	*rpoS*::*Cm* RpoS$^-$ Cm^r	This work
PPV45	*bfr*::*uidA rpoS* Bfr$^-$ RpoS$^-$ Km^r Cm^r	This work
PPV46	*bfr*::Ω-*Km ftnA*Ω-*spec* Bfr$^-$ FtnA$^-$ Km^r Spec^r	This work
PPV47	Δ*ryhB*::Ω-*spec* RyhB$^-$ Spec^r	This work
PPV48	L2 *fct*::*lacZ ftnA*Ω-*spec* Fct$^-$ Cbs$^-$ FtnA$^-$ Km^r Spec^r	This work
Escherichia coli K-12		
DH5α	*supE44* Δ*lacU169* (ϕ80*lacZ*ΔM15) *hsdR17 recA1 endA1 gyrA96 thi relA1*	48
Phage		
ϕEC2	Generalized transducing phage from *E. chrysanthemi* strain 3690	47
Plasmids		
pGEM-T Easy	3.015-kb vector, pGEM-5Zf derivative; Amp^r	Promega
pBC	3.4-kb vector, pUC19 derivative; Cm^r	Stratagene
pUIDK1	pNB4 vector carrying the *uidA*-Km cassette; Km^r Amp^r	5
pHP45Ω	pBR322 derivative carrying the Ω interposon coding for spectinomycin resistance; Amp^r Spec^r	45
pHP45Ω-Km	pHP45 derivative carrying the Ω interposon coding for kanamycin resistance; Amp^r Km^r	17
pCKC15	pUC19 derivative harboring a Cm^r cassette from plasmid pSU9 flanked by EcoRI and SmaI restriction sites	Laboratory collection
pSR2488	650-bp amplified internal fragment from the *rpoS* gene cloned into pUC18; Amp^r	This work
pTF40	1,500-bp amplified fragment of the *ftnA* gene region cloned into pGEM-T Easy; Amp^r	This work
pTF41	1,500-bp amplified fragment of the *ftnA* gene region cloned at the EcoRI site of pBC; Cm^r	This work
pTF42	Interposon Ω-Spec cloned into the MunI site of the *ftnA* gene from pTF41; Cm^r Spec^r	This work
pAB1	*uidA*-Km cassette from pUIDK1 cloned into the MunI site of the *ftnA* gene from pTF41; Cm^r Km^r	This work
pAB2	1,600-bp amplified fragment of the *bfd bfr* gene region cloned into pGEM-T Easy; Amp^r	This work
pAB3	1,600-bp amplified fragment of the *bfd bfr* gene cloned into the ApaI and SpeI sites from pBC; Cm^r	This work
pAB4	*uidA*-Km cassette from pUIDK1 cloned into the blunted PstI site of the *bfr* gene from pAB3; Cm^r Km^r	This work
pAB5	Ω-Km cassette from pHP45Ω-Km cloned into the blunted PstI site of the *bfr* gene from pAB3; Cm^r Km^r	This work
pAB6	5′ amplified region of the *ryhB* locus cloned into pGEM-T Easy; Amp^r	This work
pAB7	3′ amplified region of the *ryhB* locus cloned into pGEM-T Easy	This work
pAB8	5′ and 3′ amplified regions of the Δ*ryhB* locus cloned in pBC; Cm^r	This work
pAB9	Interposon Ω-Spec cloned into the BamHI site of the Δ*ryhB* locus from pAB8; Cm^r Spec^r	This work

ferric iron atoms for ferritins and 500 atoms for miniferritins (3, 8). These iron storage proteins possess a binuclear di-iron center that constitutes the ferroxidase center involved in the oxidation of the ferrous iron (22, 27, 28, 53). Oxygen and hydrogen peroxide are the major cellular oxidants consumed during this reaction (7, 9, 60). Ferritins can concentrate and store iron as a mineral (hydrated ferric oxide) in their central cavity (10, 25, 32). This sequestered iron is nonreactive and can serve as a reserve when the exogenous availability of this metal becomes limited. Thus, besides their role in iron storage, maxi- and miniferritins are also involved in the detoxification of this metal, dioxygen, and hydrogen peroxide under certain conditions (24, 29, 31, 54, 56, 58, 59). This work was aimed at elucidating the role of the maxiferritins in the control of iron homeostasis in *E. chrysanthemi* 3937. The results obtained show that by participating in the control of iron homeostasis, these proteins also have a role in the virulence of this bacterium.

MATERIALS AND METHODS

Bacterial strains, phage, plasmids, and media. The bacterial strains, bacteriophage, and plasmids used in this work are described in Table 1. The rich

TABLE 2. Primers used in this work

Primer	Sequence (5′–3′)[a]	Restriction site added
ftnA1s	GCTGCGTATGGTTATTTTCTG	
ftnA1r	GAAATAATCGGCGTGTATCC	
ftnA2s	CCATCAGTCACCTGCCAGTAA	
ftnA2r	GGATAATCAGCCGCCCAGCAA	
bfr1s	GGTCGTGTAGAGCGCGGCA	
bfr1r	CAGTACATAACCCCCATAT	
bfr2s	AAATGAGTTATCCGCATATGT	
bfr2r	GTGCTGACGAACGACCTGTCG	
ryhB1s	GTGGACCGCCTATACGCT	
ryhB1r	CGCGGATCCGATGAGTCACAAGGATGG	BamHI
ryhB2s	AGCGGATCCTGGTTTCCTATTTGTTTG	BamHI
ryhB2r	TCCAAAACCCTGTCCGCC	
rpoS5	CGGGATCCGGATGATCGAGAGTAAC	BamHI
rpoS6	CGGGATCCTTCAACCTGAATCTGGC	BamHI
rpoS1s	ATCACGGGTAGGAGCCACTTA	
rpoS1r	TTATTGTGCGAGTTATTCGCG	

[a] Underlining indicates the restriction site.

media used were L broth and L agar (48). To determine the effect of iron limitation on the growth of *E. chrysanthemi* cells, ethylenediamine-*N*,*N*′-bis-2-hydroxy-phenylacetic acid (EDDHA) (Sigma-Aldrich, Saint Quentin Fallavier, France) or 2,2′-dipyridyl (Sigma-Aldrich, Saint Quentin Fallavier, France) was added to L broth or L agar at a final concentration of 80 μM or 200 μM, respectively. Tris medium was used as the low-iron minimal medium (18). It was amended by adding EDDHA or 2,2′-dipyridyl at a final concentration of 40 μM or 100 μM, respectively, to achieve iron-poor conditions. For iron-rich conditions, it was supplemented with 20 μM $FeCl_3$ or 20 μM $FeSO_4$. Glucose (2 g/liter) was used as the carbon source. For genetic marker exchange by homologous recombination, minimal low-phosphate medium was used (18). *Escherichia coli* and *E. chrysanthemi* strains were grown at 37°C and 30°C, respectively. Antibacterial agents were added at the following concentrations: 50 μg/ml for ampicillin, 40 μg/ml for spectinomycin, 25 μg/ml for kanamycin, and 20 μg/ml for chloramphenicol. For oxidative growing conditions, cultures grown overnight were diluted 100-fold in L broth and grown under intensive shaking with the following compounds: 0.5 mM hydrogen peroxide (Acros Organics, Noisy le Grand, France), 6 μM paraquat (Sigma-Aldrich, Saint Quentin Fallavier, France), 2.5 μM streptonigrin (Sigma-Aldrich, Saint Quentin Fallavier, France), and 70 μM spermine NONOate (Acros Organics, Noisy le Grand, France).

Construction of ferritin-deficient mutants. Genomic fragments from the *ftnA* and *bfd-bfr* loci were amplified by PCR with the primers described in Table 2 and cloned into the pGEM-T Easy vector (Promega, Charbonnière, France). These fragments were subcloned into the pBC plasmid with appropriate restriction enzymes in order to gain unique restriction sites in the *ftnA* and *bfr* genes. The Ω interposon coding for spectinomycin resistance from pHP45Ω hydrolyzed with EcoRI was cloned into the MunI site of the *ftnA* gene, giving rise to plasmid pTF42. The Ω-Km interposon, coding for kanamycin resistance from pHP45Ω-Km hydrolyzed with SmaI, was cloned into the T4 polymerase-blunted PstI site of the *bfr* gene, giving rise to plasmid pAB5. The transcriptional *ftnA*::*uidA* and *bfr*::*uidA* fusions were constructed in vitro similarly. The *rpoS* and Δ*ryhB* mutants were constructed as follows: a 650-bp genomic internal fragment of the *rpoS* gene was amplified by PCR with primers rpoS5 and rpoS6 (Table 2). These primers contained an extra BamHI site at the 5′ ends, and the resulting PCR fragment was cloned into the BamHI site of vector pUC18, giving rise to plasmid pSR2488. The chloramphenicol resistance cartridge from pCKC15 hydrolyzed with SmaI was then introduced into the unique HpaI site located in the PCR fragment internal to the *rpoS* gene. This insertion was then introduced into the *E. chrysanthemi* chromosome by marker exchange recombination between the chromosomal allele and the plasmid-borne mutated allele. The recombinants were selected after successive cultures in low-phosphate medium in the presence of chloramphenicol, conditions in which pBR322 derivatives are very unstable. Correct recombination was confirmed by PCR and by Western blotting using anti-RpoS antibodies (data not shown). The 5′ and 3′ parts of the *ryhB* locus were PCR amplified with two couples of primers containing one degenerated primer with an extra BamHI site and cloned into the pGEM-T Easy vector. These fragments were hydrolyzed with BamHI/EcoRI or BamHI/SpeI and cloned into the pBC vector cut with EcoRI and SpeI. The Ω interposon coding for spectinomycin resistance from pHP45Ω hydrolyzed with BamHI was cloned into the BamHI site of the Δ*ryhB* gene, giving rise to plasmid pAB9. The wild-type strain of *E. chrysanthemi* was electroporated with the corresponding plasmids. Transformants were purified once on L agar plates containing the appropriate selection marker. Cultures grown with the corresponding antibiotics in L broth were 20-fold diluted in low-phosphate medium supplemented with iron in order to promote plasmid destabilization with exchange recombination of the disrupted DNA insert into the *E. chrysanthemi* chromosome. Recombinants were selected as described previously (18). The presences of disrupted *ftnA* or *bfr* genes as well a disrupted and deleted Δ*ryhB* gene in these clones were confirmed by Southern blot hybridization experiments. Double or triple mutants were constructed by using the generalized transducing phage φEC2 (47).

Determination of siderophore production, iron accumulation, and total iron content. Siderophore activities were detected as described previously (19). An iron accumulation assay was performed on 96-well culture plates. Cultures grown overnight were diluted 100-fold in wells containing L broth supplemented with 10 or 50 μM $^{55}FeSO_4$ (40 mCi · mg^{-1} iron). After 18 h of growth, cells were collected with a cell harvester (Brandel) and washed with a solution of 50 mM Tris–5 mM EDTA (pH 7.5) on filters (Wallac, Gaithersburg, MD) before scintillation counting (Trilux MicroBeta; Wallac). Whole-cell iron content was analyzed by inductively coupled plasma atomic emission spectroscopy (ICP-AES) at the Service Commun d'Analyze from Centre National de la Recherche Scientifique (Vernaison, France).

^{59}Fe labeling and preparation of whole-cell extracts. Cultures of the wild-type strain and the ferritin-deficient mutants grown overnight were diluted 100-fold in L broth and grown to an optical density at 600 nm (OD_{600}) of 0.4 when 1 μM of $^{59}FeCl_3$ (20 mCi · mg^{-1} iron) was added to the cultures. Ninety minutes after the addition of iron, cells (OD_{600} of ~1.5) were harvested by centrifugation. Cells were washed once with a solution containing 50 mM potassium phosphate (pH 7.8)–0.1 mM EDTA–10 mM $MgCl_2$ and centrifuged. Pellets were resuspended in 400 μl of the same solution in which DNase I and lysozyme were added at final concentrations of 0.1 mg/ml and 0.2 mg/ml, respectively, and incubated 30 min at 4°C. Cell lysis was achieved by six freezing/thawing cycles, and samples were kept at −20°C. Twenty-five to thirty micrograms of proteins was loaded and run on a 10% polyacrylamide nondenaturing gel. Dried gels were autoradiographed at −80°C for 12 to 24 h using Kodak (Chalon sur Saône, France) X-ray film.

Mössbauer spectroscopy. For each Mössbauer measurement, a 750-ml bacterial culture in 3-liter Erlenmeyer flasks was required in order to obtain approximately 750 μl of packed cells. Cultures of wild-type and *bfr*, *ftnA*, and *bfr ftnA* mutant strains were diluted 60-fold in Tris medium supplemented with glucose and grown to the early stationary growth phase. $[^{57}Fe(DHBA)_3]^{3-}$ was added to the cell suspensions at a final concentration of 5 μM ^{57}Fe–100 μM DHBA. Cells were grown additionally for 30, 60, and 120 min, respectively. Cells were then cooled down to 4°C within 2 min, harvested, washed in cold Tris medium, and transferred into Delrin Mössbauer sample holders. Sample volumes were about 700 μl. Sample thickness did not exceed 9 mm. The containers were quickly frozen in liquid nitrogen and kept in a liquid nitrogen storage vessel until the measurement was performed. The Mössbauer spectra were recorded in horizontal transmission geometry using a constant acceleration spectrometer operated in conjunction with a 512-channel analyzer in the time scale mode. The source was at room temperature and consisted of 0.75 GBq [^{57}Co] diffused in Rh foil (AEA, Braunschweig, Germany). The spectrometer was calibrated against a metallic α-iron foil at room temperature, yielding a standard line width of 0.24 mm/s. The Mössbauer cryostat was a helium bath cryostat (MD306; Oxford Instruments). A small field of 20 mT perpendicular to the γ-beam was applied to the tail of the bath cryostat using a permanent magnet. Isomer shift, δ, quadrupole splitting, ΔE_Q, and the percentage of the total absorption area were obtained by least-square fits of Lorentzian lines to the experimental spectra. Experiments were performed two times, and data from one experiment are shown.

General DNA methods. DNA manipulations (chromosomal DNA isolation, cloning, and electrophoresis) were described previously (18). Plasmids were extracted by using the QIAprep Spin Miniprep kit (Qiagen, Courtaboeuf, France). All cloning experiments were performed in the DH5α strain of *E. coli*. DNA/DNA hybridization analysis was performed by using Denhardt's method as described previously by Sambrook et al. (48). The primers used for PCR amplification of *E. chrysanthemi* genomic fragments are described in Table 2. PCR was performed using a DNA thermocycler (Hybaid PCR Express system) with a denaturation step at 94°C for 60 s, an annealing step at 52°C for 75 s, and an extension step at 72°C for 75 s, which was followed by an extension step at 72°C for 10 min. PCR products were cloned into the pGEM-T Easy plasmid according to the manufacturer's instructions. Nucleotide sequencing of PCR products was obtained from Genome Express (Meylan, France). For hybridization, DNA

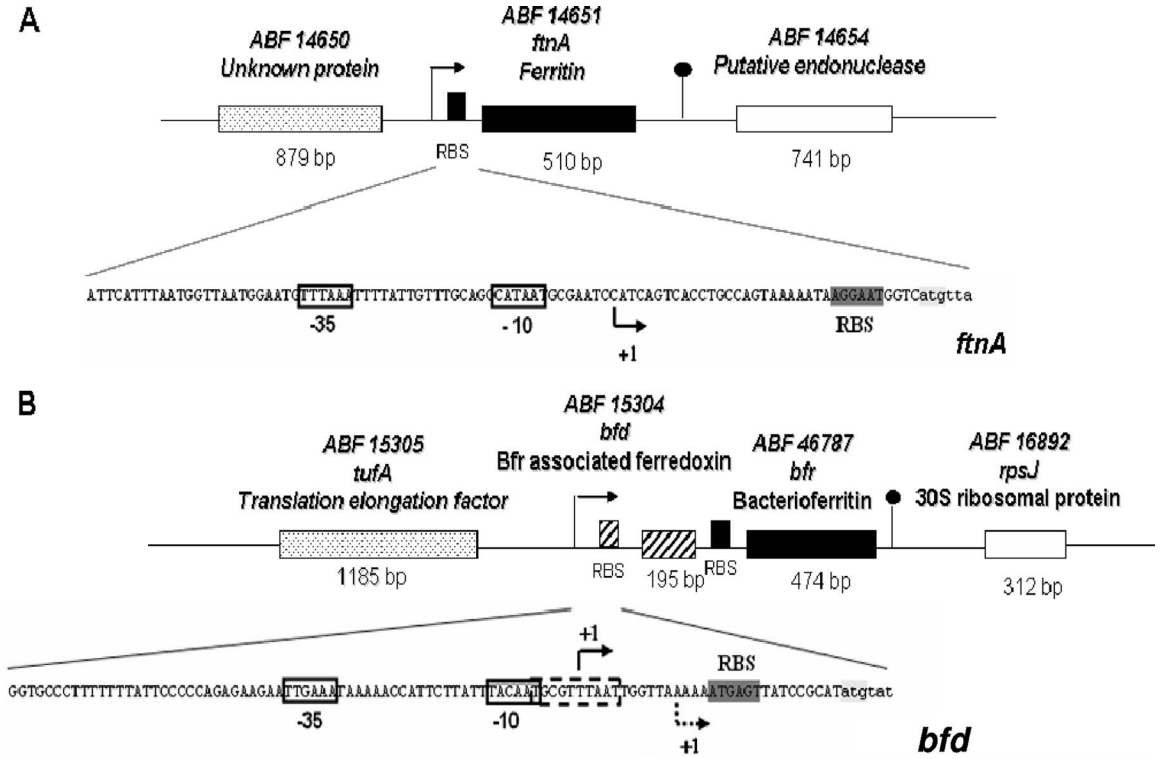

FIG. 1. Genetic organization of the loci encoding the maxiferritins FtnA (A) and Bfr (B) of *E. chrysanthemi* 3937. The −35 and −10 promoter elements are boxed. Transcriptional starts identified by primer extension experiments are indicated by an arrow. The promoter element TGCGTTTAAT of the *bfd-bfr* operon, which is similar to the RpoS factor recognition consensus sequence, is boxed with a dotted line. Inverted repeats situated at the 3′ untranslated region of the *bfr* and *ftnA* genes that may form a hairpin are indicated by a small stem-loop. The *bfr* and *ftnA* genes are transcribed in opposite directions on the chromosome. RBS, ribosome binding site.

probes were prepared by using the Prime-a-Gene labeling system according to the manufacturer's recommendations (Promega, Charbonnière, France).

RNA isolation. A culture grown overnight in L broth was diluted 60-fold in Tris medium-glucose or 100-fold in L broth. The culture was grown under shaking until an absorbance at 600 nm of 0.4 was reached, and iron (20 μM $FeSO_4$) was added or not added. A total of 7.5 ml of culture was harvested by centrifugation for 10 min at 4°C (8,000 × *g*). The cell pellet was then resuspended in 600 μl of buffer A (20 mM sodium acetate [pH 5.5], 1 mM EDTA) at 4°C. After the addition of 33 μl of 10% sodium dodecyl sulfate (SDS) and 600 μl of hot acidic phenol (65°C) equilibrated with buffer A, the sample was vigorously mixed for 30 s and incubated for 10 min at 65°C. The aqueous phase was reextracted with phenol-chloroform (1:1) equilibrated with 10 mM Tris (pH 7). RNA was precipitated overnight with 30 μl of 3 M sodium acetate and 800 μl of ethanol. The RNA pellet was washed with 70% ethanol and resuspended in 35 μl of water treated with diethyl pyrocarbonate. Northern blot analysis was performed after electrophoresis: 3 μg of RNA were loaded and run on a 1% Tris-borate-EDTA agarose gel containing 7.2% formaldehyde. After electrophoresis, RNAs were transferred onto a positively charged nylon membrane (N^+ Hybond; GE Healthcare), and hybridizations were carried out as described previously (12). Membranes were washed twice at 65°C in 5× SSC (1× SSC is 0.15 M NaCl plus 0.015 M sodium citrate)–0.5% SDS and in 1× SSC–0.5% SDS. 16S RNA was used as a control. Membranes were placed against Kodak (Chalon sur Saône, France) X-ray film at −70°C for a few days.

Determination of β-glucuronidase activities in bacterial culture. An inoculum of an L culture grown overnight was 60-fold diluted in Tris medium containing glucose or 100-fold in L broth with the appropriate antibiotics. The inoculated culture was divided into two subcultures supplemented or not with 20 μM $FeSO_4$. Cultures were grown aerobically at 30°C. Samples were collected and immediately frozen. Enzymatic activities were assayed as reported previously (51). β-Glucuronidase activity is expressed in nanomoles of paranitrophenol liberated per minute per OD_{600} unit.

Pathogenicity assays. Pathogenicity tests were performed on chicory leaves and on potted African violets (*Saintpaulia ionantha*) cv. Blue Rhapsody. Bacterial cells were plated onto L agar medium and incubated for 24 h at 30°C. Cells were suspended in an NaCl solution (9 g per liter) to give an OD_{600} of 0.4. The resulting suspension (4 μl) was used to inoculate chicory leaves, whereas 100 μl of inoculum was used for one leaf per African violet plant as described previously (51). Progression of the symptoms was scored during 4 days for the chicory test and 9 days for the *Saintpaulia* test.

RESULTS

Genetic organization of the loci encoding maxiferritins. In the genomic sequence of strain 3937, two loci encode putative maxiferritin proteins involved in iron storage: the *ftnA* and *bfr* genes encode a ferritin and a bacterioferritin, respectively (https://asap.ahabs.wisc.edu/asap). The *ftnA* gene (coding sequence [CDS] ABF-0014651) is located at position 2293752 on the *E. chrysanthemi* genome. Sequence analysis of the *ftnA* locus revealed a putative monocistronic open reading frame of 510 nucleotides encoding a 169-amino-acid polypeptide (Fig. 1A). This 19.3-kDa protein is 78% and 64% identical to the FtnA ferritins from *Yersinia pestis* KIM and *E. coli* K-12. Amino acid residues E18, Y24, E50, H53, E94, and Q127, involved in the formation of the ferroxidase site, are conserved in those proteins (53). A putative σ^{70} promoter was identified by computational analysis. For confirmation, a primer extension experiment was performed. The extension reaction product showed that the transcription of the *ftnA* gene started at a C nucleotide situated 35 bases upstream of the ATG start

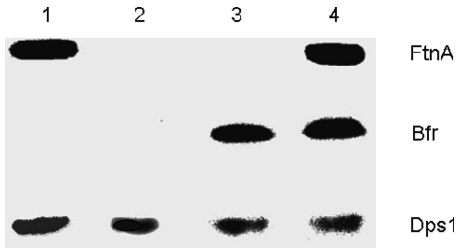

FIG. 2. Analysis of ^{59}Fe-labeled *E. chrysanthemi* proteins from soluble cell extracts after electrophoresis on a native 8% polyacrylamide gel. Bacteria were grown in L medium to an OD_{600} of 0.4, and $^{59}FeCl_3$ was added at a final concentration of 1 μM. Samples were collected 90 min after the addition of iron. Whole-cell extracts were prepared as described in Materials and Methods. The lower band probably corresponds to the Dps1 protein of *E. chrysanthemi*, as it is missing in a Dps1 gene mutant (data not shown). Lane 1, *bfr* mutant; lane 2, *bfr ftnA* mutant; lane 3, *ftnA* mutant; lane 4, wild-type strain.

codon, indicating that the anticipated promoter was functional (data not shown).

The *bfr* gene (CDS accession number ABF-0046787) appears to be clustered into an operon with the *bfd* gene (accession number ABF-0015304) (Fig. 1B). This putative polycistronic unit is located at position 4392896 on the reverse strand of the chromosome. The first gene, *bfd*, encodes a 64-amino-acid-long peptide showing 56% and 70% sequence identities with the bacterioferritin-associated [2Fe-2S] ferredoxins from *E. coli* K-12 and *Y. pestis* KIM, respectively (20). The translation start codon of the *bfr* gene is situated 53 nucleotides downstream of the end of the *bfd* gene (Fig. 1B). The *bfr* gene encodes a 157-amino-acid polypeptide that is 84% identical to the Bfr protein from *E. coli* K-12. Amino acid residues E18, Y25, E51, H54, E94, and H130, forming the ferroxidase center, are strictly conserved for both proteins (4, 53). Furthermore, methionine residue 52 of *E. coli* bacterioferritin, involved in the binding of heme, is also conserved in the Bfr protein from *E. chrysanthemi* (2). Primer extension experiments indicated that there are two transcriptional starts located 18 and 30 nucleotides upstream the of start codon of the *bfd* gene (Fig. 1B). Both promoters were predicted by computer analysis. The first one is a canonical σ^{70} promoter that can be associated with the transcription start situated ca. 30 nucleotides upstream from the ATG codon of the *bfd* gene. For the second transcriptional start, a −10 promoter element with the TGCG TTTAAT sequence could be identified. However, no −35 promoter element could be associated with this −10 region. The sequence of this −10 promoter element is reminiscent of the $TGN_{0-2}C(C/T)ATA(C/A)T$ consensus sequence identified for the *rpoS*-encoded alternative sigma factor σ^S in *E. coli* (26). At the 3′ untranslated region of the *ftnA* and *bfr* genes, inverted repeats may form a hairpin that could act as a transcription terminator.

Construction of the *bfr* and *ftnA* mutants. The *bfd-bfr* and *ftnA* loci were amplified by PCR and cloned into the pGEM-T Easy vector as described in Materials and Methods. The *bfr* and *ftnA* genes were inactivated by interposons or transcriptional *uidA* cassettes (see Materials and Methods). The disrupted *ftnA* and *bfr* genes were then introduced back into the chromosome of *E. chrysanthemi* by reverse genetics as described in Materials and Methods. The *ftnA bfr* double mutant was constructed by transducing the *ftnA* mutation into the *bfr* mutant with phage phiEC2. The presence of the disrupted genes in these mutants was confirmed by Southern experiments (data not shown). The absence of production of the FtnA and Bfr proteins in the corresponding mutants was checked by labeling exponentially growing cells with $^{59}FeCl_3$. Crude cell extracts from the wild-type strain and the *ftnA*, *bfr*, and *bfr ftnA* mutants were analyzed by native polyacrylamide gel electrophoresis as described in Materials and Methods (Fig. 2). *E. chrysanthemi* wild-type extracts showed three major bands corresponding to iron-labeled protein species (Fig. 2). The upper band was missing in the *ftnA* mutant, whereas the central band was missing in the extracts of the *bfr* mutant. Both the upper and central iron-labeled bands were not detected in the cell extracts from the double mutant, indicating that the upper and central bands correspond to the FtnA and Bfr proteins, respectively.

Growth characteristics of the *E. chrysanthemi bfr*, *bfr ftnA*, and *ftnA* mutants. We checked the growth properties of the ferritin-deficient mutants in L broth and in the low-iron minimal Tris medium. In L medium, the growth of the *ftnA* mutant was slower than that of the wild-type strain, giving rise to a final cellular density lower than that of the wild-type strain (data not shown). The decrease in the growth yield of the *ftnA* mutant was more important in Tris medium (Table 3). The addition of iron to Tris medium stimulated the growth of the *ftnA* mutant and the wild-type strain. However, the growth of the *ftnA* mutant still remained affected compared to that of the wild type (Table 3). The addition of the iron chelator EDDHA or 2,2′-dipyridyl to Tris medium severely reduced the growth capacity of the *ftnA* mutant in comparison to that of the wild-type strain. The intracellular ferrous iron chelator 2,2′-dipyridyl gave the highest inhibitory effect (Table 3). Under all growth conditions tested, the *bfr* mutant behaved like the wild-type strain, whereas the *bfr ftnA* double mutant displayed an intermediate growth phenotype (Table 3). The introduction of plasmid pTF41, containing the wild-type *ftnA* gene in the *ftnA* mutant, restored its growth capacity in the presence of the iron chelators (data not shown). The altered growth capacity of the *ftnA* mutant under conditions of iron starvation indicates that the absence of a functional ferritin alters the ability of the bacterium to overcome iron deprivation. On L agar plates, colony development was slower for the *ftnA* mutant than for the wild-type strain and other ferritin-deficient mutants. Under

TABLE 3. Growth capacity of the *E. chrysanthemi* ferritin-deficient mutants compared to the wild-type strain in Tris medium with different iron avalaibilities[a]

Mutant	Ratio of final cell density of mutant/final cell density of wild type ± SD			
	Tris medium	+ Fe	+ EDDHA	+ Dipyridyl
ftnA	0.74 ± 0.03	0.80 ± 0.03	0.69 ± 0.03	0.63 ± 0.03
bfr	1	1	1	1
bfr ftnA	0.90 ± 0.02	0.91 ± 0.02	0.88 ± 0.03	0.87 ± 0.03

[a] Ratios of the final cellular density of the mutants to that of the wild-type strain are given. Three experiments were performed, and standard deviations are shown.

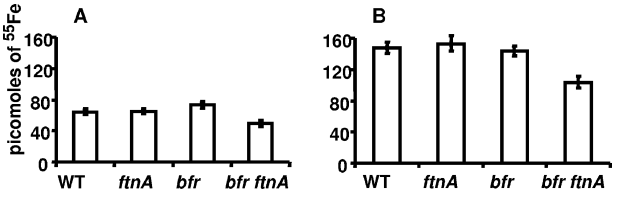

FIG. 3. Iron accumulation in the wild-type strain and the ferritin-deficient mutants of *E. chrysanthemi*. Bacteria were grown overnight in L broth with 10 μM (A) or 50 μM (B) $FeSO_4$. Cells were harvested on filters and washed as described in Materials and Methods. The amounts of ^{55}Fe taken up by cells of the wild-type (WT) strain and the different ferritin-deficient mutants are indicated in picomoles of iron per OD_{600} unit. Experiments were performed in triplicate, and standard deviations are shown.

anaerobic conditions, only the *ftnA* mutant showed a reduced growth yield (data not shown).

Iron transport, whole-cell iron content, and Mössbauer spectroscopy. The absence of functional ferritins can change the intracellular iron pool distribution and thus can lead to the metallation and activation of the Fur repressor. Therefore, we analyzed the production of siderophores, chrysobactin and achromobactin (44, 39), in the *bfr*, *ftnA*, and *bfr ftnA* mutants grown in Tris medium. Kinetics and levels of achromobactin and chrysobactin production were almost identical for the wild-type strain and the ferritin-deficient mutants (data not shown). We also found that the transcription of biosynthetic genes for achromobactin or chrysobactin was not reduced in these mutants (data not shown).

As the lack of functional ferritins could reduce the ability of bacteria to save iron when this metal becomes abundant, we checked the capacities of the different ferritin mutants to store iron by growing cells overnight in L medium supplemented with 1, 10, or 50 μM $^{55}FeSO_4$. For 1 μM iron, the wild-type strain and the different ferritin mutants accumulated the same quantity of iron (data not shown). Amounts of ^{55}Fe taken up and stored by the cells increased with increasing concentrations of this metal (Fig. 3A and B). For both iron concentrations, there was no significant difference in the amount of iron taken up by the wild-type strain and the *bfr* or the *ftnA* mutant (Fig. 3A and B). However, the *bfr ftnA* double mutant accumulated less iron than the wild-type strain (Fig. 3A and B). This defect in iron accumulation was more pronounced at the highest $FeSO_4$ concentration tested. Indeed, the double mutant accumulated 20% less iron than the wild-type strain at an $FeSO_4$ concentration of 10 μM and 33% less iron at a concentration of 50 μM (Fig. 3A and B). These data were corroborated by analyzing the total Fe content in the wild-type and ferritin-deficient mutant strains by ICP-AES. In L medium supplemented with 50 μM $FeCl_3$, only the double mutant displayed a decrease of 30% in the total amount of intracellular iron in comparison to the iron content of the wild-type strain and the *bfr* and *ftnA* mutants (data not shown).

The natures of the intracellular iron pools of the wild-type strain and the mutants were analyzed by in situ Mössbauer spectroscopy. In principle, in situ Mössbauer spectroscopy enables the simultaneous identification of all main iron metabolites on a qualitative level as well as on a quantitative level without the destruction of cellular assembly (35, 36). Cells were grown in Tris medium to the beginning of the stationary phase in order to achieve a high bacterial yield. A ferric complex of 2,3-dihydroxybenzoic acid, $[^{57}Fe(DHBA)_3]^{3-}$, was added to the culture, and 30, 60, and 120 min after the addition of this complex, cells were collected and prepared as described in Materials and Methods. Figure 4A displays Mössbauer spectra from cells of the *E. chrysanthemi* wild-type strain and its ferritin-deficient mutants after 120 min of incubation, which is the time when ferritin signals are easily observed (46). Mössbauer parameters of the spectra are listed in Table 4. The spectrum of the ferric DHBA complex (not shown here) displays a broad six-line pattern dominated by spin-spin relaxation, like other catecholate complexes at 77 K. Since such a spectrum is lacking in the cell spectra, it is safe to state that iron of this complex has been metabolized. The spectra exhibit two quadrupole doublets. One doublet corresponds to high-spin ferrous iron in an octahedral oxygen or nitrogen environment. Such a component has been observed in many bacterial systems. In *E. coli*, it was shown that this component is located in the cytoplasm and corresponds to an oligomeric ferrous sugar-phosphate complex (6). The second component represents a ferric high-spin species exhibiting Mössbauer parameters similar to those of a variety of bacterial ferritins. Figure 4B displays the Mössbauer spectra of the *bfr ftnA* mutant and the wild-type strain measured at 2 K. At this temperature, ferric iron of the wild-type strain displays magnetic broadening, and the doublet disappears. This feature was described previously (46) and is typical of bacterial ferritins. In contrast, the double mutant shows a ferric iron doublet even at 2 K, indicating the different natures of the two ferric iron components. The spectra of the wild-type strain and the *bfr* mutant exhibit very similar features (Fig. 4A). The majority of metabolized iron is found in FtnA (approximately 70%), and a smaller portion is ferrous iron (approximately 30%). In both strains, the overall iron incorporation is very similar, as estimated from the absolute areas. The most striking difference between the spectra of *ftnA* and *bfr ftnA* mutants compared to those of wild-type and *bfr* strains is the ferrous iron/ferric iron ratios, which are 1.65 and 1.98, respectively (Table 4). Both mutants are lacking a functional *ftnA* gene. The large contribution of Fe^{2+} reflects a lack of proper storage due to the absence of the ferritin FtnA. Moreover, Bfr is obviously not a replacement for FtnA. Therefore, the function of the bacterioferritin is not storage of bulk iron, indicating that Bfr is probably not involved in the regular iron storage transfer $2Fe^{2+} + 1/2O_2 + 2H_2O + \text{FtnA} + (H_2PO_4)^- \rightarrow (Fe_2O_3H_3\ PO_4)\ \text{FtnA} + 3H^+$. In addition, the observed excess of Fe^{2+} in spectra of the *ftnA* and *bfr ftnA* mutants indicates an impaired balance of general iron metabolism after $[^{57}Fe(DHBA)_3]^{3-}$ uptake (Fig. 4A). Due to the lack of *bfr* and *ftnA* genes in the double mutant, the ferric iron contribution cannot be attributed to the maxiferritin Bfr or FtnA. Rather, we suggest that this species represents ferric Dps. We further assume that the same is true for the *ftnA* mutant.

Sensitivity of the ferritin mutants to oxidative stress. Since the intracellular iron pool could contribute to oxidative stress, we checked the sensitivities of ferritin mutants to hydrogen peroxide and to compounds generating the superoxide ion O_2^- (paraquat), radicals (streptonigrin), and nitric oxide (spermine NONOate). The addition of these compounds to L medium

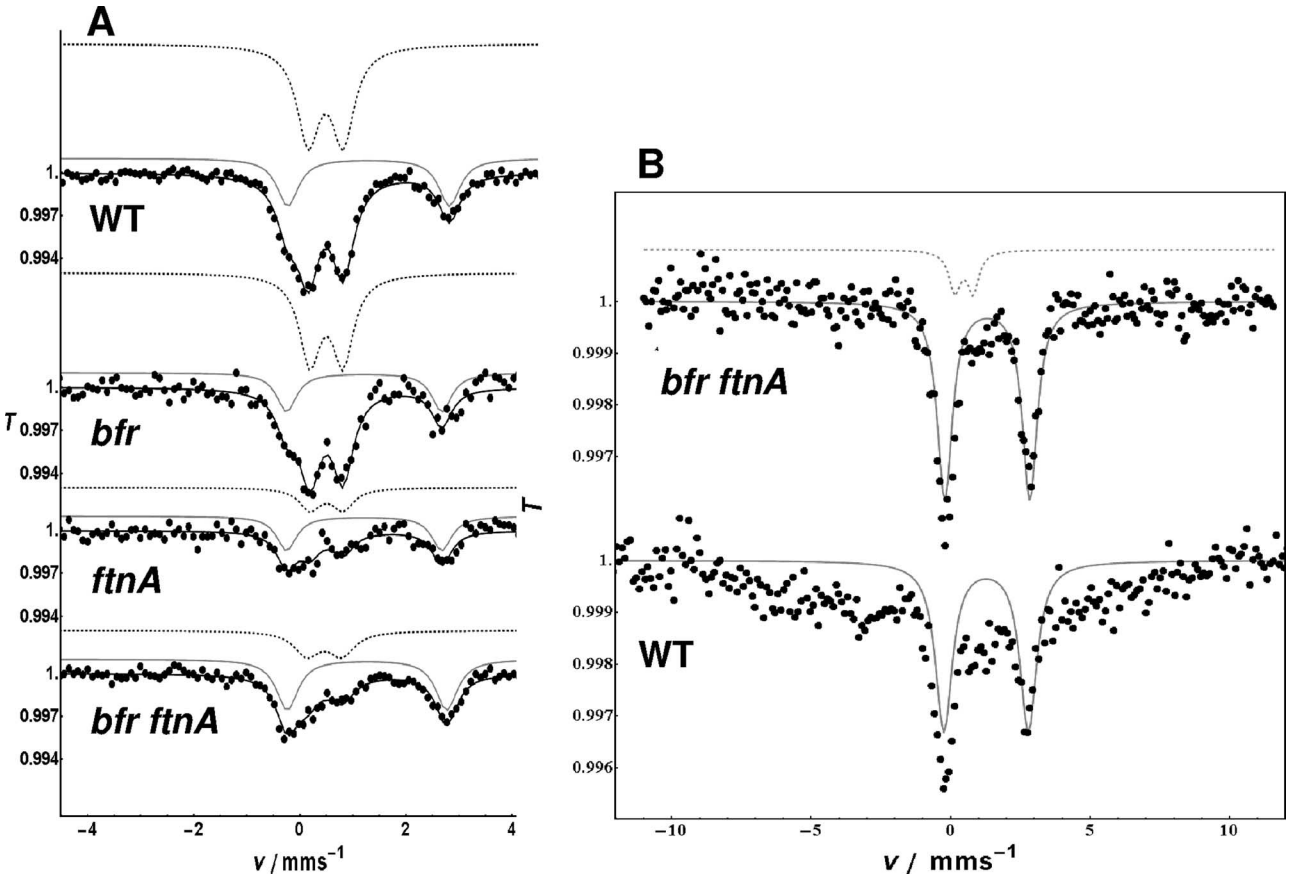

FIG. 4. Mössbauer spectra of *Erwinia chrysanthemi* 3937 cells measured at 77 K (A) and 2 K (B). *T* represents the relative transmission, and *v* represents the energy scale measured as the velocity in mm/s. Genotypes of the different strains are indicated on the spectra. Cells were grown to an OD_{600} of 0.8 and incubated for 120 min with 5 μM ^{57}Fe–100 μM DHBA. (A) Each spectrum is characterized by two quadrupole doublets, the parameters of which are listed in Table 4. The dashed gray line corresponds to the least-square fits of ferric high-spin iron to the experimental spectra, and full gray lines correspond to ferrous high spin. (B) Mössbauer spectra from cells of the *bfr ftnA* double mutant and the wild-type (WT) strain of *E. chrysanthemi* 3937 measured at 2 K. In both spectra, a ferrous high-spin component is observed (full gray lines). In the double mutant, the ferric ion doublet is still visible at 2 K (dashed gray line), whereas in the wild-type strain, this component broadens at temperatures below 4.3 K due to magnetic splitting, and the doublet disappears. The magnetic splitting is not resolved due to relaxation effects and was not fitted.

impaired the growth of the *ftnA* mutant (Fig. 5). The wild-type strain and the *bfr* mutant displayed the same sensitivities to all these compounds (Fig. 5). In addition, the *bfr ftnA* double mutant was sensitive to streptonigrin only. The introduction of plasmid pTF41, containing the wild-type *ftnA* gene, enabled the *ftnA* mutant to grow in the presence of these oxidative stress-generating compounds (data not shown). Thus, the increased sensitivity of the *ftnA* mutant to oxidative stress is caused by the lack of a functional ferritin.

TABLE 4. Mössbauer parameters of spectra of early-stationary-phase *E. chrysanthemi* cells after 120 min of incubation with $[Fe(DHBA)_3]^{3-}$ determined by least-square fits of Lorentzian lines

Strain	δ (mm s^{-1})	ΔE_Q (mm s^{-1})	Γ (mm s^{-1})	Area (%)	Fe(II)/Fe(III) ratio
Wild type (ferrous)	1.30	3.05	0.48	32.6	0.48
Wild type (ferric)	0.49	0.66	0.50	67.4	
bfr (ferrous)	1.21	2.93	0.45	29.7	0.42
bfr (ferric)	0.48	0.63	0.48	70.3	
ftnA (ferrous)	1.27	2.93	0.35	62.3	1.65
ftnA (ferric)	0.51	0.78	0.31	37.7	
bfr ftnA (ferrous)	1.26	3.01	0.50	66.5	1.98
bfr ftnA (ferric)	0.48	0.65	0.50	33.5	

Pathogenicity of the ferritin mutants. We examined the behaviors of the ferritin mutants of strain 3937 after inoculation onto chicory leaves. In comparison with the wild-type strain, the *ftnA*, *bfr*, and *bfr ftnA* mutants displayed a delay in the appearance of symptoms of maceration (Fig. 6A). However, once symptoms started, the progression of mutants and that of the wild-type strain were the same. For potted African violets, a lag in the appearance of maceration symptoms was observed only for the *ftnA* mutant (Fig. 6B). One week after inoculation, the numbers of systemic responses for the wild-type strain and those of its *ftnA* derivative mutant were identical (Fig. 6B). The *bfr* and *bfr ftnA* mutants were as virulent as the wild-type strain on African violets (data not shown). The delay in symptom appearance for the *ftnA* mutant is consistent with the fact that this mutant is sensitive to iron starvation and to oxidative stress, which are conditions encountered by bacterial cells during infection. Since symptom evolution for the wild-type strain

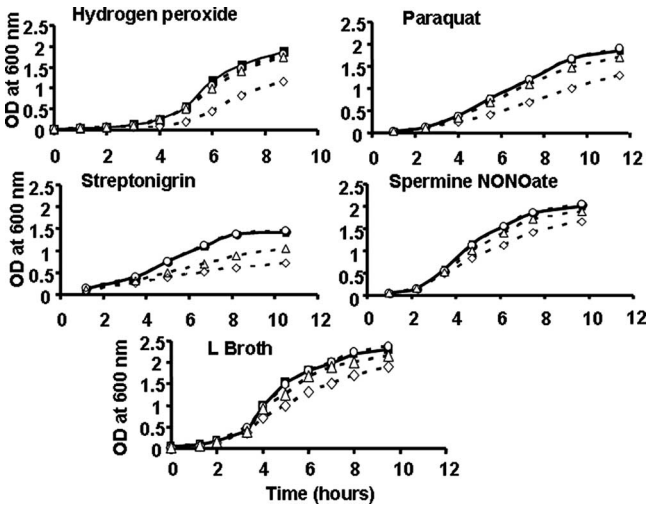

FIG. 5. Growth of the wild-type strain and the ferritin-deficient mutants of *E. chrysanthemi* under oxidative and nitrosative conditions. Cells were grown in L medium with intensive shaking under normal conditions or in the presence of 0.5 mM of H_2O_2, 6 μM paraquat, 2.5 μM streptonigrin, or 70 μM spermine NONOate, as indicated on the graphs. Filled squares, wild-type strain; open circles, *bfr* mutant; open diamonds, *ftnA* mutant; open triangles, *bfr ftnA* mutant. Experiments were performed five times, and the data reported are the means of three independent experiments, with standard deviations corresponding to less than 5%.

was similar to that of the *ftnA* mutant, we analyzed the global production of pectate lyases in this mutant grown in Tris medium with polygalacturonic acid as a carbon source. This in vitro condition mimics the plant environment, where low iron availability triggers pectate lyase production (18, 51). The level of pectate lyase production was 2.5 higher for the *ftnA* mutant than for the wild-type strain (data not shown). This higher production of pectinases could enable the *ftnA* mutant to multiply in planta despite its lower growth capacity and its increased sensitivity to oxidative stress. Indeed, destruction of plant cells by pectate lyases increases nutrient and iron availability and limits the activation of the plant cell NADPH oxidase (16).

Regulation of the *ftnA* gene. Since the *ftnA* gene is devoted to iron storage, we first examined its expression after the addition of iron. Cells harboring a transcriptional *ftnA*::*uidA* fusion were grown in L broth, and $FeSO_4$ was added to a final concentration of 20 μM at an optical density of 0.5. Exogenous iron increased *ftnA* gene transcription fourfold (data not shown). In many enterobacteria, the iron control of the *ftnA* gene is mediated by the small antisense RNA RyhB (33). We identified a homologue of the *E. coli ryhB* gene in the *E. chrysanthemi* 3937 genome. The *E. chrysanthemi ryhB* gene (CDS accession number ABF-0061312) encodes a 120-nucleotide-long RNA, which may be untranslated. Potential −10 and −35 promoter elements were predicted by computational analysis. This promoter region is highly similar to that of the *E. coli ryhB* gene, with a putative Fur box matching the consensus sequence at 17 out of 19 positions which overlaps the −10 promoter element (Fig. 7A). Although the *E. chrysanthemi* RyhB RNA is longer than that of *E. coli*, the last 75 nucleotides are conserved in both RNAs (92% identity). We found sequence complementarity between the *E. chrysanthemi* RyhB RNA and the 5′ end of the *ftnA* gene that includes the 5′ leader sequence with the potential translational starts of the *ftnA* RNA (Fig. 7B). We constructed a Δ*ryhB* mutant by reverse genetics (see Materials and Methods). Increased *ftnA* transcript levels were detected in total RNA isolated from the Δ*ryhB* strain in comparison to RNAs isolated from the wild-type strain (Fig. 7C). RyhB RNA abundance was notably increased under conditions of iron starvation (Fig. 8A). Furthermore, the *ryhB* gene is highly expressed in a *fur* mutant regardless of the iron concentration (Fig. 8B), and this high level of transcription greatly decreased the amount of *ftnA* RNA, as shown in Fig. 8C. Thus, in *E. chrysanthemi*, the control of *ftnA* gene expression involves the transcriptional repressor Fur and a homolog of the small antisense RNA RyhB.

Regulation of the *bfd-bfr* operon. Since RyhB expression reduces *bfr* transcript abundance in *E. coli* (34), we first investigated whether the small RNA RyhB could pair to the *E. chrysanthemi bfd* and *bfr* genes. No sequence complementarity was detected between the polycistronic *bfd-bfr* transcript and

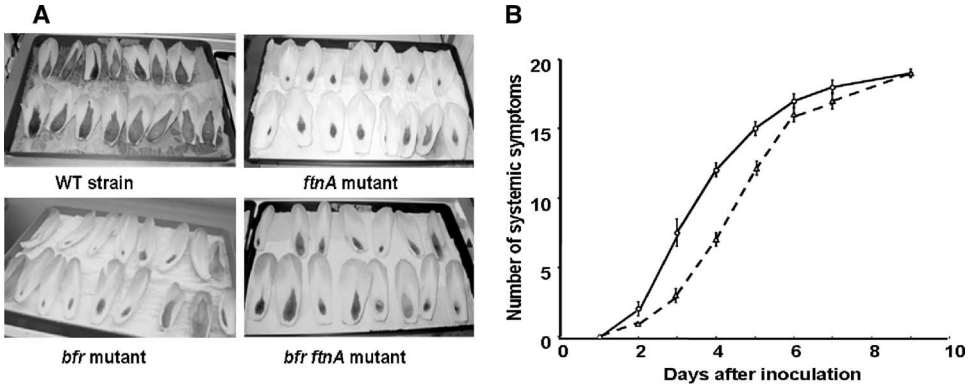

FIG. 6. Pathogenicity of the wild-type strain and its ferritin-negative mutants. (A) Symptoms caused by *Erwinia chrysanthemi* strain 3937 and its ferritin-deficient mutants on chicory leaves 36 h postinoculation. (B) Pathogenicities of the wild-type (WT) strain (solid line) and the *ftnA* mutant (dashed line) on African violets. The progression of systemic symptoms (i.e., fully macerated leaf and petiole) was scored for 9 days as indicated. Experiments were performed in triplicate, and standard deviations are shown.

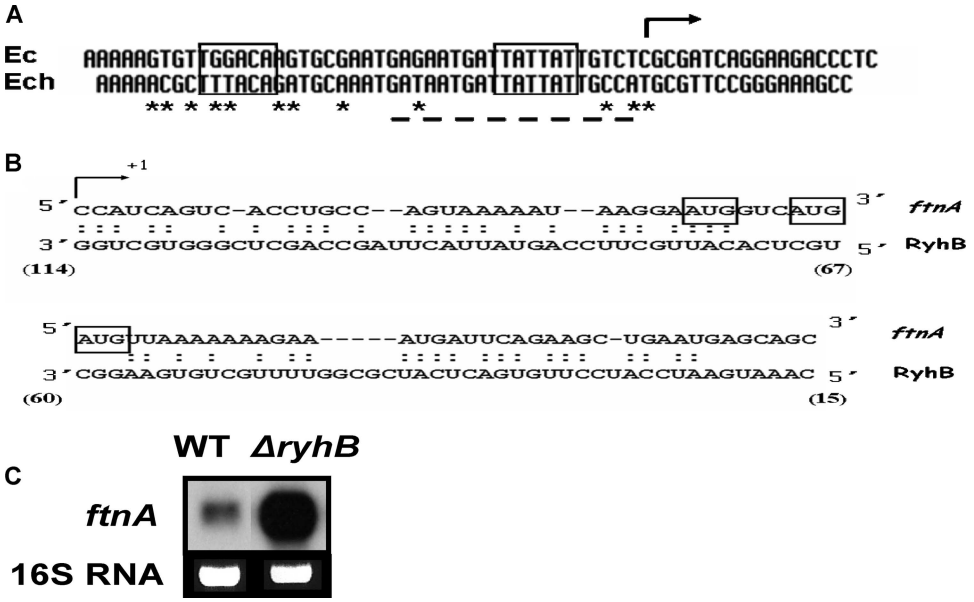

FIG. 7. Occurrence of a *ryhB* gene in *E. chrysanthemi*. (A) Sequence alignment of the promoters of the *ryhB* genes of *E. coli* (Ec) and *E. chrysanthemi* 3937 (Ech). The −35 and −10 promoter elements are boxed, and the potential Fur box is underlined. The transcriptional start identified in *E. coli* is indicated by an arrow. Nonconserved nucleotides are indicated by asterisks. (B) Sequence complementarity between the *E. chrysanthemi* RyhB RNA and the 5′ part of the *ftnA* transcript. The identified transcriptional start of the *ftnA* gene is indicated by an arrow, and the potential translational starts are boxed. Numbers indicate nucleotide positions in RyhB RNA. (C) Northern blot analysis of *E. chrysanthemi ftnA* messenger accumulation in the wild-type (WT) strain and the Δ*ryhB* mutant. Total RNAs were extracted from cells at the late exponential growth phase, and 3 μg of RNA was blotted as described in Materials and Methods. Northern blot analysis was performed as described in Materials and Methods.

RyhB RNA. Northern blot experiments corroborated this computational analysis by showing that the level of transcription of the *bfd-bfr* operon in the wild-type strain was identical to that in the Δ*ryhB* mutant (Fig. 9A). Interestingly, in L broth, the expression of the *bfr*::*uidA* transcriptional fusion seemed to be dependent on cellular density since the highest expression occurred at the beginning of the stationary phase (Fig. 9B). Thus, we checked whether quorum sensing was implicated in this control. Transcription of the *bfd-bfr* operon in the wild-type strain was identical to that in the *expR* or *canR* mutant, which are altered in quorum-sensing regulation (data not shown). Since the σ^S transcription factor was shown to be involved in the regulation of the *bfr* gene in *E. coli* (26), we checked this possibility in *E. chrysanthemi*. We thus transduced the *bfr*::*uidA* fusion into an *rpoS* mutant of *E. chrysanthemi* 3937. In an *rpoS* genotype, the transcription of the *bfd-bfr* operon was reduced to a basal level, even at a high cellular density (Fig. 10A). Indeed, very low levels of *bfr* RNA were detected by Northern blot hybridization in total RNAs isolated from the *E. chrysanthemi rpoS* mutant (Fig. 10B). McHugh et al. (38) previously demonstrated that the Fur transcriptional repressor was involved in the regulation of the *bfd-bfr* operon in *E. coli*. We also examined the role of the Fur repressor in the expression of the *bfd-bfr* operon. In a *fur* genotype, there was only a very low level of transcription of the *bfr* gene (Fig. 11A). Since the *E. chrysanthemi fur* mutant is altered in its growth capacity and displays a lower final cellular density than that of the wild-type strain (18), we checked the levels of the *rpoS* gene transcripts in this mutant. As shown in Fig. 11B, there was a lower level of accumulation of *rpoS* transcripts in RNAs

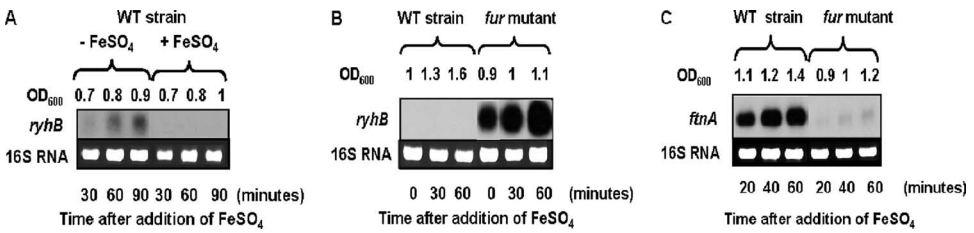

FIG. 8. Northern blot analyses of *ryhB* and *ftnA* gene expression in *E. chrysanthemi*. (A) The wild-type (WT) strain was grown in Tris medium until an OD_{600} of 0.7 was reached, and 20 μM $FeSO_4$ was added. Samples were collected every 30 min. (B) RyhB RNA accumulation in the wild-type strain of *E. chrysanthemi* and its Fur^- derivative. Cells were grown in L broth until an OD_{600} of 1 was reached, and 20 μM $FeSO_4$ was added. Samples were collected every 30 min. (C) *ftnA* messenger accumulation in the wild-type strain and the *fur* mutant. Cells were grown in L broth until an OD_{600} of 1 was reached, and 20 μM $FeSO_4$ was added. Samples were collected every 20 min. Northern experiments were performed as described in Materials and Methods.

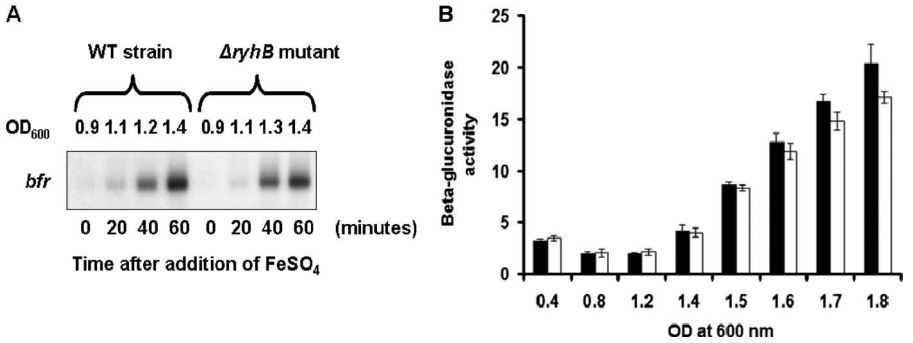

FIG. 9. Analysis of *bfr* gene expression in *E. chrysanthemi.* (A) *bfr* messenger accumulation in the wild-type (WT) strain and the Δ*ryhB* mutant. Cells were grown in L broth until an OD_{600} of 0.9 was reached, and 20 μM $FeSO_4$ was added. Samples were collected every 20 min, and Northern experiments were carried out as described in Materials and Methods. (B) Expression of a transcriptional *bfr*::*uidA* fusion during bacterial growth. Cells were grown in L medium. $FeSO_4$ (20 μM) was added at an OD_{600} of 0.4. Samples were collected after the addition of iron as indicated. β-Glucuronidase activity was determined as described in Materials and Methods. White bars, with iron; black bars, no iron. Experiments were performed in triplicate, and standard deviations are shown.

isolated from the *fur* mutant. In this mutant, the pattern of *rpoS* RNA accumulation correlated with the observed level of transcription of the *bfr* gene. Thus, in a *fur* mutant, the reduced level of expression of the *bfr* gene is likely caused by a decreased accumulation of the *rpoS* RNA.

DISCUSSION

In this work, we investigated the physiological roles of the *E. chrysanthemi* ferritin protein FtnA and bacterioferritin protein Bfr in iron storage. We show that the Bfr and FtnA proteins participate in different steps of iron storage in *E. chrysanthemi*. Relevantly, the different role of these proteins appears to be related to a differential regulation of expression of their genes.

In contrast to *E. coli* and *Salmonella enterica* serovar Typhimurium, strain 3937 of *E. chrysanthemi* harbors only two maxiferritins, since the *ftnB* locus is missing in its genome. The FtnB protein is a nonubiquitous ferritin-like protein that lacks the typical amino acids that form the ferroxidase center (1, 57). We constructed the *ftnA*, *bfr*, and *bfr ftnA* mutants by reverse genetics, and we characterized their phenotypes. No clear phenotype could be assigned to the *bfr* mutation. Indeed, this mutant behaved like the wild-type strain under conditions of iron deficiency or under oxidative stress conditions. Experiments measuring the total cellular iron content and Mössbauer analysis of the intracellular iron pool showed that Bfr plays no significant role in iron storage at stationary phase in *E. chrysanthemi*. This is in contrast to the role of the Bfr protein from *Salmonella enterica* serovar Typhimurium, which is an important iron reservoir and is implicated in resistance to H_2O_2 stress (57). Nevertheless, the *E. chrysanthemi bfr* mutant was less aggressive on chicory leaves, with a delay in the appearance of symptoms of maceration. Thus, the role of bacterioferritin in iron homeostasis in *E. chrysanthemi* remains to be elucidated.

As is the case in *E. coli*, the main iron storage protein in *E. chrysanthemi* 3937 is the ferritin FtnA (1). The absence of a functional FtnA leads to a pleiotropic phenotype. In comparison to the wild-type strain, growth of the *ftnA* mutant was impaired even in the presence of iron. This mutant is also more sensitive to iron deficiency than the wild-type strain. An increased sensitivity to compounds generating oxidative and nitrosative stress was also observed for the *ftnA* mutant. Interestingly, the *ftnA* mutant also grew less well under anaerobic conditions (data not shown). Thus, the reduced growth ability

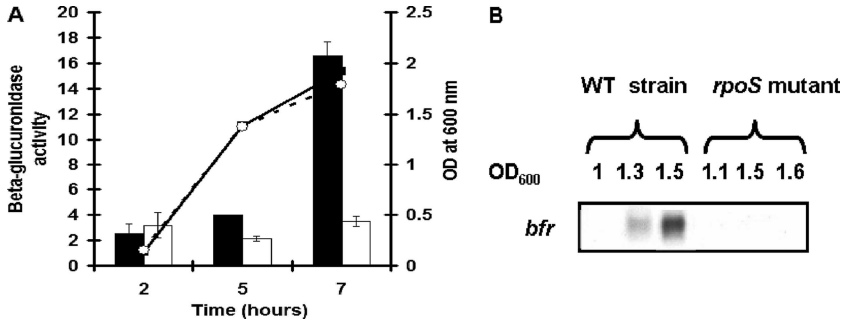

FIG. 10. Effect of an *rpoS* mutation on the expression of the *E. chrysanthemi bfr* gene. (A) Expression of a transcriptional *bfr*::*uidA* fusion in the wild-type strain and the *rpoS* mutant. Bacterial growth in L broth was assessed by measuring the OD_{600} (filled squares, *bfr*::*uidA* mutant; open circles, *bfr*::*uidA rpoS* mutant). β-Glucuronidase activity was determined as described in Materials and Methods. Black bars, *bfr*::*uidA* mutant; white bars, *bfr*::*uidA rpoS* mutant. Experiments were performed in triplicate, and standard deviations are shown. (B) *bfd-bfr* messenger accumulation in the wild-type (WT) strain and the *rpoS* mutant. Cells were grown in L medium, and samples were collected during growth. Northern blot analysis was performed as described in Materials and Methods.

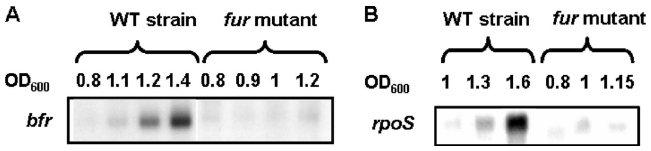

FIG. 11. Effect of a *fur* mutation on the expression of the *bfr* and *rpoS* genes of *E. chrysanthemi*. (A) *bfr* messenger accumulation in the wild-type (WT) strain and the *fur* mutant. (B) Expression of the *rpoS* gene in the wild-type strain and the *fur* mutant. Bacteria were grown in L medium and collected during growth as indicated by the OD_{600}. *bfr* and *rpoS* transcripts were detected by Northern blot analysis as described in Materials and Methods.

of this mutant not only is caused by the sensitivity to oxidative stress but is also a direct consequence of a lack of the FtnA-associated iron store. Increases in the ferrous iron/ferric iron ratio in the *ftnA* mutant, as determined by Mössbauer analysis, are probably the cause of its sensitivity to oxidative stress. Interestingly, inactivation by mutations of the high-affinity iron transport systems decreased the susceptibility of the *ftnA* mutant to oxidative stress (data not shown). Thus, by limiting the intracellular concentration of ferrous iron and reducing the cytotoxic effect of Fenton's chemistry, FtnA confers tolerance to oxygen metabolism in *E. chrysanthemi*. Surprisingly, the *bfr ftnA* double mutant is less susceptible to iron starvation than the *ftnA* mutant. In addition, the *bfr ftnA* mutant is sensitive only to oxidative stress caused by streptonigrin. However, its susceptibility is intermediate to those of the wild-type strain and the *ftnA* mutant. One explanation could be that there is a reduction in the total iron content of the double ferritin mutant as determined by the ICP-AES analysis. Although there is a higher Fe(II)/Fe(III) ratio, the decrease in the total iron content of this mutant could account for its intermediate phenotype. Analysis of Mössbauer spectra from the *bfr ftnA* mutant clearly demonstrated an Fe(III) signal that could be attributed to the ferric iron stored in Dps proteins. Indeed, we identified two genes encoding Dps proteins in the genome of *E. chrysanthemi* strain 3937. In the absence of maxiferritins, these proteins would limit the intracellular concentration of reactive iron by sequestering an excess of this metal. Another nonexclusive hypothesis might be that in an *ftnA* background, the absence of a functional Bfr results in changes in iron distribution in proteins or other components. The physiological consequences of the combination of the *ftnA* and *bfr* mutations on iron homeostasis remain to be determined.

The control of *ftnA* and *bfr* gene expression in *E. chrysanthemi* is similar to the regulation occurring in *E. coli*. Iron is a triggering signal for transcription to the *ftnA* gene. This control involves the Fur transcriptional repressor and a small RNA that is a functional homolog of the *E. coli* RyhB antisense RNA. *E. chrysanthemi* RNA is longer than that of *E. coli* (i.e., 120 versus 90 nucleotides). However, both RNAs show significant sequence identity in their last 80 nucleotides. This RNA possesses a long sequence complementarity with the 5′ end of the *ftnA* transcript, suggesting a base-pairing mechanism of regulation similar to that described previously for *E. coli* (33). Indeed, in a Δ*ryhB* mutant, we observed an elevated level of the *ftnA* transcript. We also showed that the *ryhB* gene is negatively controlled by Fur. Thus, in a *fur* mutant, there was a very low level of the *ftnA* transcript in total RNA because of the overaccumulation of RyhB. No sequence complementarity between RyhB RNA and the *bfd-bfr* operon could be found. Our Northern experiments showed that the transcription of the *bfd-bfr* operon is not controlled by RyhB RNA. A high level of transcription of this operon was observed at the beginning of the stationary phase, and we found that quorum sensing is not involved in this regulatory process. The σ^S factor mediates this response, since transcription of the *bfd-bfr* operon was reduced in a *rpoS* mutant. This result is in agreement with the σ^S-regulated promoter that we identified for the *bfd-bfr* operon. Surprisingly, the expression of the *bfd-bfr* operon was also strongly decreased in a *fur* mutant. This regulatory response is probably indirect, since no potential Fur binding site was identified in the *bfd-bfr* operon sequence. However, we showed that there was a delay in the accumulation of the *rpoS* transcript in a *fur* mutant. This lower *rpoS* transcript level can account for the reduced expression of the *bfd-bfr* operon in the *fur* mutant. The mechanisms by which Fur modulates the transcription of *rpoS* or the stability of its RNA must be determined.

Mutations in the *ftnA* and *bfr* genes had different consequences on the virulence of *E. chrysanthemi*. All the ferritin-deficient mutants are less aggressive on chicory leaves, whereas only the *ftnA* mutant displayed a reduced virulence on African violets. These data are similar to those obtained for the *E. chrysanthemi suf* mutants, which are affected in the Suf machinery involved in the biogenesis/repair of the Fe-S centers under iron deficiency and oxidative conditions (41). Indeed, a *sufA* mutant lacking the [Fe-S] scaffold protein SufA is less virulent than the wild-type strain only on chicory leaves. A *sufC* mutant where the SufC ATPase component of the SufBCD complex is missing is altered in its pathogenicity to isolated organs and potted African violets. Our explanation may be that iron availability and oxidative stress conditions are different depending on the host tissues infected. Thus, under infection conditions where the environment is continually changing, a perfect control of iron homeostasis is important for *E. chrysanthemi* cells. In conclusion, although the *E. chrysanthemi* FtnA and Bfr proteins are highly similar to those of *E. coli* and *S. enterica*, their physiological roles seem to be different. When bacteria possess multiple maxiferritins, the respective functions of these proteins in the control of iron and dioxygen chemistry may depend on the iron metabolism machinery and the ecophysiology of the species.

ACKNOWLEDGMENTS

We thank Jan Schorch for technical assistance. We are grateful to the reviewers for their suggestions to improve the manuscript.

This work was supported by the Institut National de la Recherche Agronomique (project SPE 0217-01) and the Procope program (grant 09636TF) from the Ministère des Affaires Etrangères. D. Expert is a researcher from the CNRS. A. Boughammoura was supported by a doctoral fellowship from the Ministère de l'Education Nationale, de l'Enseignement Supérieur, et de la Recherche.

REFERENCES

1. **Abdul-Tehrani, H., A. J. Hudson, Y. S. Chang, A. R. Timms, C. Hawkins, J. M. Williams, P. M. Harrison, J. R. Guest, and S. C. Andrews.** 1999. Ferritin mutants of *Escherichia coli* are iron deficient and growth impaired, and *fur* mutants are iron deficient. J. Bacteriol. **181:**1415–1428.
2. **Andrews, S. C., N. E. Le Brun, V. Barynin, A. J. Thomson, G. R. Moore, J. R. Guest, and P. M. Harrison.** 1995. Site-directed replacement of the coaxial heme ligands of bacterioferritin generates heme-free variants. J. Biol. Chem. **270:**23268–23274.

3. **Andrews, S. C., A. K. Robinson, and F. Rodriguez-Quinones.** 2003. Bacterial iron homeostasis. FEMS Microbiol. Rev. **27:**215–237.
4. **Baaghil, S., A. Lewin, G. R. Moore, and N. E. Le Brun.** 2003. Core formation in *Escherichia coli* bacterioferritin requires a functional ferroxidase center. Biochemistry **42:**14047–14056.
5. **Bardonnet, N., and C. Blanco.** 1992. *uidA*-antibiotic resistance cassettes for insertion mutagenesis, gene fusions and genetic constructions. FEMS Microbiol. Lett. **93:**243–248.
6. **Böhnke, R., and B. F. Matzanke.** 1995. The mobile ferrous iron pool in *E. coli* is bound to a phosphorylated sugar derivative. Biometals **8:**223–230.
7. **Bou-Abdallah, F., A. C. Lewin, N. E. Le Brun, G. R. Moore, and N. D. Chasteen.** 2002. Iron detoxication properties of *Escherichia coli* bacterioferritin. Attenuation of oxyradical chemistry. J. Biol. Chem. **277:**37064–37069.
8. **Carrondo, M. A.** 2003. Ferritins, iron uptake and storage from the bacterioferritin viewpoint. EMBO J. **22:**1959–1968.
9. **Ceci, P., A. Ilari, E. Falvo, and E. Chiancone.** 2003. The Dps protein of *Agrobacterium tumefaciens* does not bind to DNA but protects it toward oxidative cleavage: X-ray crystal structure, iron binding, and hydroxyl-radical scavenging properties. J. Biol. Chem. **278:**20319–20326.
10. **Chasteen, N. D., and P. M. Harrison.** 1999. Mineralization in ferritin: an efficient means of iron storage. J. Struct. Biol. **126:**182–194.
11. **Chiancone, E., P. Ceci, A. Ilari, F. Ribacchi, and S. Stefanini.** 2004. Iron and proteins for iron storage and detoxification. Biometals **17:**197–202.
12. **Dellagi, A., M. Rigault, D. Segond, C. Roux, Y. Kraepiel, F. Cellier, J. F. Briat, F. Gaymard, and D. Expert.** 2005. Siderophore-mediated upregulation of Arabidopsis ferritin expression in response to *Erwinia chrysanthemi* infection. Plant J. **43:**262–272.
13. **El Hassouni, M., J. P. Chambost, D. Expert, F. Van Gijsegem, and F. Barras.** 1999. The minimal gene set member *msrA*, encoding peptide methionine sulfoxide reductase, is a virulence determinant of the plant pathogen *Erwinia chrysanthemi*. Proc. Natl. Acad. Sci. USA **96:**887–892.
14. **Enard, C., A. Diolez, and D. Expert.** 1988. Systemic virulence of *Erwinia chrysanthemi* 3937 requires a functional iron assimilation system. J. Bacteriol. **170:**2419–2426.
15. **Expert, D.** 1999. Withholding and exchanging iron: interactions between Erwinia ssp. and their plant hosts. Annu. Rev. Phytopathol. **37:**307–334.
16. **Fagard, M., A. Dellagi, C. Roux, C. Périno, M. Rigault, V. Boucher, V. Shevchik, and D. Expert.** 2007. *Arabidopsis thaliana* expresses multiple lines of defense to counter-attack *Erwinia chrysanthemi*. Mol. Plant-Microbe Interact. **20:**794–805.
17. **Fellay, R., J. Frey, and H. M. Krisch.** 1987. Interposon mutagenesis of soil and water bacteria: a family of DNA fragments designed for in vitro insertional mutagenesis of gram-negative bacteria. Gene **52:**147–154.
18. **Franza, T., C. Sauvage, and D. Expert.** 1999. Iron regulation and pathogenicity in *Erwinia chrysanthemi* strain 3937: role of the Fur repressor protein. Mol. Plant-Microbe Interact. **12:**119–129.
19. **Franza, T., B. Mahé, and D. Expert.** 2005. *Erwinia chrysanthemi* requires a second iron transport route dependent of the siderophore achromobactin for extracellular growth and plant infection. Mol. Microbiol. **55:**261–275.
20. **Garg, R. P., C. J. Vargo, X. Cui, and D. M. Kurtz, Jr.** 1996. A [2Fe-2S] protein encoded by an open reading frame upstream of the *Escherichia coli* bacterioferritin gene. Biochemistry **35:**6297–6301.
21. **Hugouvieux-Cotte-Pattat, N., and J. Robert-Baudouy.** 1985. Lactose metabolism in *Erwinia chrysanthemi*. J. Bacteriol. **162:**248–255.
22. **Ilari, A., S. Stefanini, E. Chiancone, and D. Tsernoglou.** 2000. The dodecameric ferritin from Listeria innocua contains a novel intersubunit iron-binding site. Nat. Struct. Biol. **7:**38–43.
23. **Imlay, J. A.** 2006. Iron-sulphur clusters and the problem with oxygen. Mol. Microbiol. **59:**1073–1082.
24. **Ishikawa, T., Y. Mizunoe, S. Kawabata, A. Takade, M. Harada, S. N. Wai, and S. Yoshida.** 2003. The iron-binding protein Dps confers hydrogen peroxide stress resistance to *Campylobacter jejuni*. J. Bacteriol. **185:**1010–1017.
25. **Kauko, A., A. T. Pulliainen, S. Haataja, W. Meyer-Klaucke, J. Finne, and A. C. Papageorgiou.** 2006. Iron incorporation in *Streptococcus suis* Dps-like peroxide resistance protein Dpr requires mobility in the ferroxidase center and leads to the formation of a ferrihydrite-like core. J. Mol. Biol. **364:**97–109.
26. **Lacour, S., and P. Landini.** 2004. σ^S-dependent gene expression at the onset of stationary phase in *Escherichia coli*: function of σ^S-dependent genes and identification of their promoter sequences. J. Bacteriol. **186:**7186–7195.
27. **Le Brun, N. E., S. C. Andrews, J. R. Guest, P. M. Harrison, G. R. Moore, and A. J. Thomson.** 1995. Identification of the ferroxidase centre of *Escherichia coli* bacterioferritin. Biochem. J. **312:**385–392.
28. **Liu, X., and E. C. Theil.** 2004. Ferritin reactions: direct identification of the site for the diferric peroxide reaction intermediate. Proc. Natl. Acad. Sci. USA **101:**8557–8562.
29. **Liu, X., K. Kim, T. Leighton, and E. C. Theil.** 2006. Paired *Bacillus anthracis* Dps (mini-ferritin) have different reactivities with peroxide. J. Biol. Chem. **281:**27827–27835.
30. **Luo, Y., Z. Han, S. M. Chin, and S. Linn.** 1994. Three chemically distinct types of oxidants formed by iron-mediated Fenton reactions in the presence of DNA. Proc. Natl. Acad. Sci. USA **91:**12438–12442.
31. **Ma, J. F., U. A. Ochsner, M. G. Klotz, V. K. Nanayakkara, M. L. Howell, Z. Johnson, J. E. Posey, M. L. Vasil, J. J. Monaco, and D. J. Hasset.** 1999. Bacterioferritin A modulates catalase A (KatA) activity and resistance to hydrogen peroxide in *Pseudomonas aeruginosa*. J. Bacteriol. **181:**3730–3742.
32. **Mann, S., J. M. Williams, A. Treffry, and P. M. Harrison.** 1987. Reconstituted and native iron-cores of bacterioferritin and ferritin. J. Mol. Biol. **198:**405–416.
33. **Massé, E., and S. Gottesman.** 2002. A small RNA regulates the expression of genes involved in iron metabolism in *Escherichia coli*. Proc. Natl. Acad. Sci. USA **99:**4620–4625.
34. **Massé, E., C. K. Vanderpool, and S. Gottesman.** 2005. Effect of RyhB small RNA on global iron use in Escherichia coli. J. Bacteriol. **187:**6962–6971.
35. **Matzanke, B. F.** 1987. Mössbauer spectroscopy of microbial iron uptake and metabolism, p 251–284. *In* G. Winkelmann, D. van der Helm, and J. B. Neilands (ed.), Iron transport in microbes, plants and animals. Verlag Chemie, Weinheim, Germany.
36. **Matzanke, B. F.** 1991. Structures, coordination chemistry and functions of microbial iron chelates, p 15–60. *In* G. Winkelmann (ed.), Handbook of microbial iron chelates (siderophores). CRC Press, Boca Raton, FL.
37. **Matzanke, B. F.** 1997. Iron storage in microorganisms, p. 117–158. *In* G. Winkelmann, and C. J. Carrano, (ed.), Transition metals in microbial metabolism. Harwood Academic Publishers GmbH, Amsterdam, The Netherlands.
38. **McHugh, J. P., F. Rodriguez-Quinones, H. Abdul-Tehrani, D. A. Svistunenko, R. K. Poole, C. E. Cooper, and S. C. Andrews.** 2003. Global iron-dependent gene regulation in Escherichia coli. A new mechanism for iron homeostasis. J. Biol. Chem. **278:**29478–29486.
39. **Münzinger, M., H. Budzikiewicz, D. Expert, C. Enard, and J. M. Meyer.** 2000. Achromobactin, a new citrate siderophore of Erwinia chrysanthemi. Z. Naturforsch. C **55:**328–332.
40. **Murdoch, L., J. C. Corbel, D. Reis, Y. Bertheau, and B. Vian.** 1999. Differential cell wall degradation by Erwinia chrysanthemi in petiole of Saintpaulia ionantha. Protoplasma **210:**59–74.
41. **Nachin, L., M. El Hassouni, L. Loiseau, D. Expert, and F. Barras.** 2001. SoxR-dependent response to oxidative stress and virulence of Erwinia chrysanthemi: the key role of SufC, an orphan ABC ATPase. Mol. Microbiol. **39:**960–972.
42. **Nachin, L., L. Loiseau, D. Expert, and F. Barras.** 2003. SufC: an unorthodox cytoplasmic ABC/ATPase required for [Fe-S] biogenesis under oxidative stress. EMBO J. **22:**427–437.
43. **Pérombelon, M. C. M.** 2002. Potato diseases caused by soft rot erwinias: an overview of pathogenesis. Plant Pathol. **51:**1–12.
44. **Persmark, M., D. Expert, and J. B. Neilands.** 1989. Isolation, characterization and synthesis of chrysobactin, a compound with a siderophore activity from Erwinia chrysanthemi. J. Biol. Chem. **264:**3187–3193.
45. **Prentki, P., and H. M. Krisch.** 1984. In vitro insertional mutagenesis with a selectable DNA fragment. Gene **29:**303–313.
46. **Rauscher, L., D. Expert, B. F. Matzanke, and A. X. Trautwein.** 2002. Chrysobactin-dependent iron acquisition in Erwinia chrysanthemi: functional study of an homologue of the Escherichia coli ferric enterobactin esterase. J. Biol. Chem. **277:**2385–2395.
47. **Résibois, A., M. Colet, M. Faelen, E. Schoonejans, and A. Toussaint.** 1984. Phi-EC2 a new generalized transducing phage of Erwinia chrysanthemi. Virology **137:**102–112.
48. **Sambrook, J., E. F. Fritsch, and T. Maniatis.** 1989. Molecular cloning: a laboratory manual, 2nd ed. Cold Spring Harbor Laboratory Press, Cold Spring Harbor, NY.
49. **Samson, R., J. B. Legendre, R. Christen, M. Fischer-Le Saux, W. Achouak, and L. Gardan.** 2005. Transfer of Pectobacterium chrysanthemi (Burkholder et al. 1953, Brenner et al. 1973) and Brenneria paradisiaca to the genus Dickeya gen. nov. as Dickeya chrysanthemi comb. nov. and Dickeya paradisiaca comb. nov. and delineation of four novel species, Dickeya dadantii sp. nov., Dickeya dianthicola sp. nov., Dickeya dieffenbachiae sp. nov., and Dickeya zeae sp. nov. Int. J. Syst. Evol. Microbiol. **55:**1415–1427.
50. **Santos, R., T. Franza, M. L. Laporte, C. Sauvage, D. Touati, and D. Expert.** 2001. Essential role of superoxide dismutase on the pathogenicity *of Erwinia chrysanthemi* strain 3937. Mol. Plant-Microbe Interact. **14:**758–767.
51. **Sauvage, C., and D. Expert.** 1994. Differential regulation by iron of Erwinia chrysanthemi pectate lyases: pathogenicity of iron transport regulatory *cbr* mutants. Mol. Plant-Microbe Interact. **7:**71–77.
52. **Smith, J. L.** 2004. The physiological role of ferritin-like compounds in bacteria. Crit. Rev. Microbiol. **30:**173–185.
53. **Stillman, T. J., P. P. Connolly, C. L. Latimer, A. F. Morland, M. A. Quail, S. C. Andrews, A. J. Hudson, A. Treffry, J. R. Guest, and P. M. Harrison.** 2003. Insights into the effects on metal binding of the systematic substitution of five key glutamate ligands in the ferritin of Escherichia coli. J. Biol. Chem. **278:**26275–26286.
54. **Theil, E. C., M. Matzapetakis, and X. Liu.** 2006. Ferritins: iron/oxygen biominerals in protein nanocages. J. Biol. Inorg. Chem. **11:**803–810.
55. **Toth, I. K., K. S. Bell, M. C. Holeva, and P. R. J. Birch.** 2003. Soft rot erwiniae: from genes to genomes. Mol. Plant Pathol. **4:**17–30.
56. **Ueshima, J., M. Shoji, D. B. Ratnayake, K. Abe, S. Yoshida, K. Yamamoto,**

and K. Nakayama. 2003. Purification, gene cloning, gene expression, and mutants of Dps from the obligate anaerobe *Porphyromonas gingivalis*. Infect. Immun. **71:**1170–1178.
57. **Velayudhan, J., M. Castor, A. Richardson, K. L. Main-Hester, and F. C. Fang.** 2007. The role of ferritins in the physiology of *Salmonella enterica* sv. Typhimurium: a unique role for ferritin B in iron-sulphur cluster repair and virulence. Mol. Microbiol. **63:**1495–1507.
58. **Wang, G., Y. Hong, A. Olczak, S. E. Maier, and R. J. Maier.** 2006. Dual roles of *Helicobacter pylori* NapA in inducing and combating oxidative stress. Infect. Immun. **74:**6839–6846.
59. **Yamamoto, Y., M. Higuchi, L. B. Poole, and Y. Kamio.** 2000. Role of the *dpr* product in oxygen tolerance in *Streptococcus mutans*. J. Bacteriol. **82:**3740–3747.
60. **Zhao, G., P. Ceci, A. Ilari, L. Giangiacomo, T. M. Laue, E. Chiancone, and N. D. Chasteen.** 2002. Iron and hydrogen peroxide detoxification properties of DNA-binding protein from starved cells. A ferritin-like DNA-binding protein of Escherichia coli. J. Biol. Chem. **277:**27689–27696.